RESEARCH

Rate-induced tipping can trigger plankton blooms

Anna Vanselow[1] · Lukas Halekotte[1,2] · Pinaki Pal[3] · Sebastian Wieczorek[4] · Ulrike Feudel[1]

Abstract

Plankton blooms are complex nonlinear phenomena whose occurrence can be described by the two-timescale (fast-slow) phytoplankton-zooplankton model introduced by Truscott and Brindley (*Bulletin of Mathematical Biology* 56(5):981–998, 1994). In their work, they observed that a sufficiently fast rise of the water temperature causes a critical transition from a low phytoplankton concentration to a single outburst: a so-called plankton bloom. However, the dynamical mechanism responsible for the observed transition has not been identified to the present day. Using techniques from geometric singular perturbation theory, we uncover the formerly overlooked rate-sensitive quasithreshold which is given by special trajectories called *canards*. The transition from low to high concentrations occurs when this rate-sensitive quasithreshold moves past the current state of the plankton system at some narrow *critical range of warming rates*. In this way, we identify *rate-induced tipping* as the underlying dynamical mechanism of largely unpredictable plankton blooms such as red tides, or more general, harmful algal blooms. Our findings explain the previously reported transitions to a single plankton bloom, and allow us to predict a new type of transition to a sequence of blooms for higher rates of warming. This could provide a possible mechanism of the observed increased frequency of harmful algal blooms.

Keywords Plankton blooms · Predator-prey models · Slow-fast systems · Rate-induced tipping · Canard trajectory · Transient dynamics

✉ Anna Vanselow
anna.vanselow@uol.de

Lukas Halekotte
lukas.halekotte@uol.de

Pinaki Pal
pinaki.math@gmail.com

Sebastian Wieczorek
sebastian.wieczorek@ucc.ie

Ulrike Feudel
ulrike.feudel@uol.de

1 Institute for Chemistry and Biology of the Marine Environment, Carl von Ossietzky University Oldenburg, Carl von Ossietzky-Str. 9-11, Oldenburg 26111, Germany

2 German Aerospace Center, Institute for the Protection of Terrestrial Infrastructures, Rathausallee 12, Sankt Augustin 53757, Germany

3 Department of Mathematics, National Institute of Technology, Durgapur 713209, West Bengal, India

4 School of Mathematical Sciences, University College Cork, Western Road, Cork T12XF64, Ireland

Introduction

Marine phytoplankton do not only form the basis of marine food webs and provide approximately half of the global primary production, they also contribute to essential biogeochemical processes in the ocean (Field et al. 1998; Falkowski 2012). A striking feature of many phytoplankton populations is the occurrence of so-called plankton blooms — a phenomenon characterized by a rapid increase in plankton concentrations followed by an almost equally rapid decline. Plankton blooms can occur seasonally (e.g., spring blooms) or in a more erratic fashion (e.g., red tides). A potentially catastrophic situation occurs when some of the bloom-forming species release toxic chemicals which can paralyze or even kill some affected marine species (Amaya et al. 2018; Griffith et al. 2019). The corresponding blooms are called harmful algal blooms (HABs).

In the past, various drivers of both types of blooms have been identified. Regarding spring blooms, the role of light and mixing processes has been emphasized for many decades (Gran and Braarud 1935; Riley 1946; Riley et al. 1949; Sverdrup 1953). The certainly most prominent hypothesis

regarding the driving factor is the so-called *critical depth hypothesis* which has already been suggested in the middle of the last century (Gran and Braarud 1935; Sverdrup 1953) and which can still be found in more recently published textbooks (Simpson and Sharples 2012). Its key element constitutes the *critical mixing depth* above which improved upper ocean growth conditions allow for the accumulation of phytoplankton and thus ultimately for the formation of plankton blooms. Later, the role of biotic factors such as grazing pressure (Behrenfeld 2010; Behrenfeld et al. 2013), competition (Chakraborty and Feudel 2014; Busch et al. 2019), viral infection and parasitism (Chambouvet et al. 2008; Velo-Suárez et al. 2013; Richards 2017) or community composition (Lewandowska et al. 2015) attracted increasing attention. These studies include the *disturbance-recovery hypothesis* proposed by Behrenfeld (2010). The hypothesis presumes that blooms are initiated by recurring physical processes that disrupt the balance between phytoplankton reproduction and grazer consumption. According to the work of Behrenfeld and colleagues, this imbalance is caused by the annual deepening of the mixed layer which "dilutes" the grazing pressure on the phytoplankton which, in turn, allows for its significant accumulation (Behrenfeld 2010; Behrenfeld and Boss 2014).

In contrast to spring blooms, red tides or harmful algal blooms are more localized outbreaks which are not strongly correlated with a particular seasonal change in the upper ocean growth conditions. However similar to spring blooms, it is assumed that red tides occur due to an imbalance that affects the major contributing factors to phytoplankton growth: increasing light availability, rising temperature, nutrient enrichment and the reduction of the grazing pressure (Chakraborty and Feudel 2014; Truscott and Brindley 1994; Winder et al. 2012; Lewandowska et al. 2014; Hjerne et al. 2019; Trombetta et al. 2019; Sommer and Lewandowska 2011).

In order to fully understand the mechanisms underlying the emergence of annually occurring spring blooms and less predictable HABs such as red tides, it is not only important to identify the environmental conditions that induce the imbalance, but also to describe how this imbalance emerges. Interestingly, the magnitude of environmental change may not be the one decisive factor for the onset of a plankton bloom, which could disclose why the full explanation of this phenomenon has been elusive. The rate of change of environmental conditions also appears to play an important role (Pinek et al. 2020). The indications of rate dependence come from a study in which the Helgoland Roads long-term data series are analyzed (Freund et al. 2006). The study reveals that the spring bloom onset is correlated with a rapid increase of temperature, and not so much with the temperature itself.

The speed of temperature increase also plays a decisive role in the formation of red tides in the theoretical work of Truscott and Brindley (1994). Inspired by the idea of an excitable medium capable of mimicking fast growing harmful plankton blooms, they formulate a plankton model which consists of a fast evolving phytoplankton population that is controlled by a much slower reproducing zooplankton population. Depending on the speed of temperature increase, their time-scaled model shows two disparate transient behaviors: (i) balance of phytoplankton and zooplankton at low plankton densities (Fig. 1a) or (ii) the formation of a single plankton bloom (Fig. 1b). They further ascertain that both behaviors are delimited by a specific value of the speed of temperature increase ($v \approx 0.003$ in Fig. 1). However, they were not able to identify the *rate-sensitive quasithreshold* that separates these two very different transient responses to temperature increase. In other words, the trigger mechanism of the harmful algal bloom has not been identified.

Mathematically, the model of Truscott and Brindley (1994) consists of one fast variable, the phytoplankton, and

Fig. 1 The phytoplankton (P)-zooplankton (Z) model developed by Truscott and Brindley (1994) is sensitive to rates of environmental change v. It changes its dynamics from the stationary coexistence of P and Z at low densities. **a** to the sudden formation of a phytoplankton bloom **b** if solely the growth rate of the phytoplankton increases faster than the rate $v \approx 0.003$ day^{-1} (as response to increasing temperatures). The phytoplankton density is displayed in green and red while the zooplankton density is shown in gray
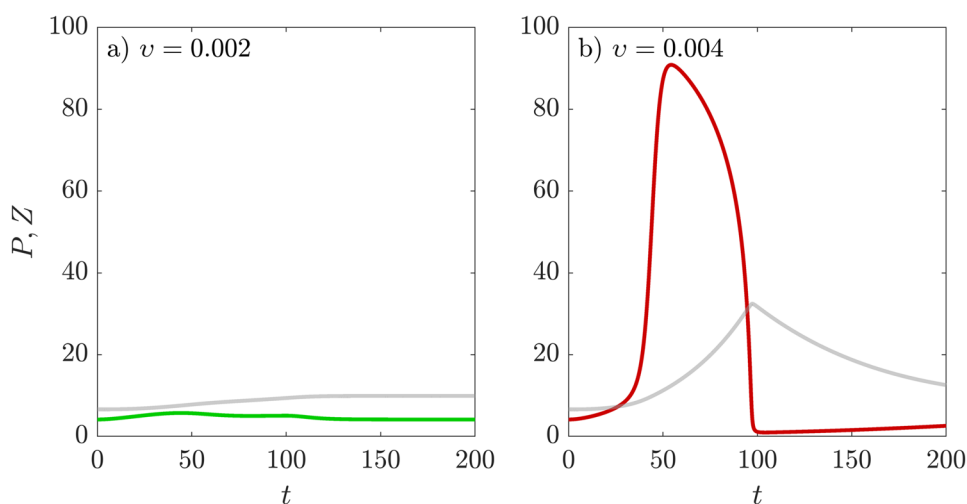
two slow variables, the zooplankton and the time-varying environmental condition which changes at a given rate. In such two-timescale systems, exceptional solutions called *canards* are typical (Benoît [1981], [1983]; Dumortier and Roussarie [1996]; Szmolyan and Wechselberger [2001]), and form boundaries between different dynamical regimes (Wieczorek et al. [2011]; Wechselberger et al. [2013]; Perryman and Wieczorek [2014]). For instance, canards can separate small-amplitude oscillations from relaxation oscillations (Brøns et al. [2008]; Desroches et al. [2012]), different types of spiking behavior in neuronal models (Izhikevich [2007]; Mitry et al. [2013]), different states of CO_2-concentration in the atmosphere (Wieczorek et al. [2011]; O'Sullivan et al. [2022]), or disparate transient (Vanselow et al. [2019]) or asymptotic (O'Keeffe and Wieczorek [2020]) dynamics in biological systems characterized by different dominating species. In the latter four examples, similar to the observations of Truscott and Brindley ([1994]), a variation of the rate of environmental change alone can cause a transition from one dynamical regime to another by crossing canard solutions. These critical transitions have been classified as *rate-induced tipping points* by Ashwin et al. ([2012]). Others identified so-called *folded-saddle* canards as non-obvious thresholds for the onset of rate-induced tipping (Wieczorek et al. [2011]; Mitry et al. [2013]; Perryman and Wieczorek [2014]; O'Sullivan et al. [2022]). Specifically, as the rate of environmental change increases, the position of the rate-dependent threshold shifts in state space and might pass the current state of the system, giving rise to a large nonlinear response. It is important to note that in these cases there is no classical bifurcation (no loss of stability in the classical autonomous sense), such as the dangerous saddle-node bifurcation, separating different dynamical regimes. Instead, the different dynamical regimes are solely separated by rate-sensitive canard solutions.

In this work, we uncover the rate-sensitive boundary, that is the singular canard solution, in the model of Truscott and Brindley ([1994]). Furthermore, we demonstrate that this boundary gives rise to a quasithreshold for rate-induced tipping, which is the dynamical mechanism responsible for the observed harmful algal blooms (Fig. [1]). To this end, we start by introducing the phytoplankton-zooplankton model of Truscott and Brindley ([1994]) (Sec. "The model"). Afterwards, we reproduce their simulations in which the phytoplankton population is exposed to rapidly increasing growth rates induced by increasing temperatures. Then, we study the resulting rate-sensitive dynamics using geometric singular perturbation theory, and reveal the singular canard solution (Sec. "Rate-induced tipping triggers plankton bloom"). Moreover, we show that, depending on the location of the singular canard, the model can show more than one sequentially occurring plankton bloom (Sec. "R-tipping can trigger two sequentially occurring plankton blooms"). Next, we relate this singular canard to a family of canards that form a quasithreshold. Finally, we discuss our results (Sec. "Discussion").

The model

The Truscott-Brindley model (Truscott and Brindley [1994]) (in the following the TB-model) combines a logistic growth of a phytoplankton population P, a zooplankton population Z growing by the Holling-type III functional response (Holling [1959a], [b]), and dying with standard linear mortality.

$$\frac{dP}{d\tau} = r\,P\left(1 - \frac{P}{K}\right) - R_m\,Z\,\frac{P^2}{\alpha^2 + P^2} := f(P, Z, r), \qquad (1)$$

$$\frac{dZ}{d\tau} = \gamma\,R_m\,Z\,\frac{P^2}{\alpha^2 + P^2} - \mu\,Z := g(P, Z). \qquad (2)$$

In the following, we vary exclusively the growth rate r of the phytoplankton population while the other parameters are kept constant. The constant parameters K, R_m, α, γ and μ represent the carrying capacity of the phytoplankton population, the attack rate, the half-saturation phytoplankton concentration, the conversion efficiency and the mortality rate of zooplankton population (see Table [1] for the parameter values).

We will analyze the response of the plankton model to a gradual increase of the phytoplankton growth rate r, which could be caused by a gradual increase in temperature. Specifically, we consider the simplest case in which r increases linearly over time at a rate η as long as $r \in (r_{min}, r_{max})$, and remains constant when $r = r_{min}$ or $r = r_{max}$ (Fig. [2]a):

$$\frac{dr}{d\tau} = \begin{cases} \eta > 0 & \text{if } r_{min} < r < r_{max}, \\ 0 & \text{if } r = r_{min} \text{ or } r_{max}. \end{cases} \qquad (3)$$

In the extended TB-model [(1)](3), the phytoplankton population P evolves on a different time scale than its grazer Z. This can be demonstrated by transforming the model into a non-dimensional form, which we show in detail in Appendix [A.1]. Considering the non-dimensional TB-model Eqs. [(A5)], [(A6)] and [(A9)], it becomes apparent that the time scale separation is determined by the

Table 1 Parameter values of the TB-model [(1)](3) according to Truscott and Brindley ([1994])

Parameter	Value
Carrying capacity K	108 μg N l^{-1}
Attack rate zooplankton R_m	0.7 day^{-1}
Half-saturation constant α	5.7 μg N l^{-1}
Conversion efficiency γ	0.05
Mortality rate zooplankton μ	0.012 day^{-1}
Minimum growth rate r_{min}	0.2 day^{-1}
Maximum growth rate r_{max}	0.6 day^{-1}
$P(0) = P_0$	$e_P\mu$g N l^{-1}
$Z(0) = Z_0$	$e_Z\mu$g N l^{-1}
$r(0) = r_0$	0.4 day^{-1}
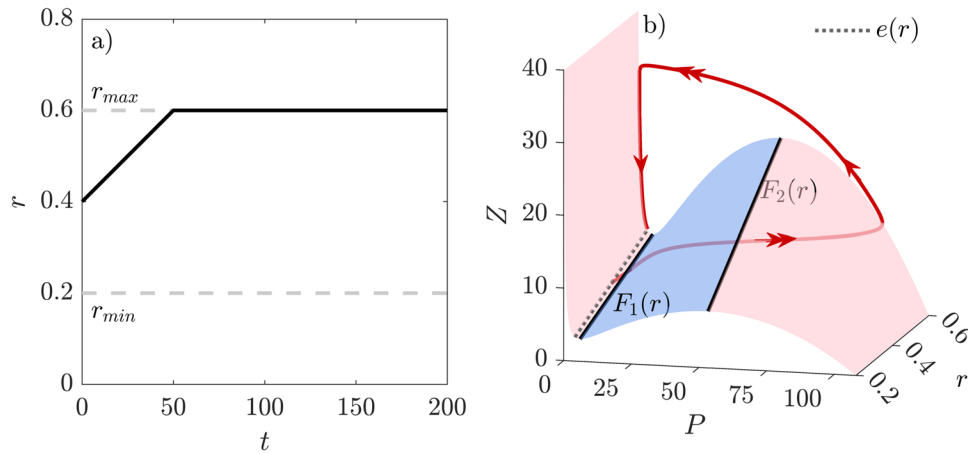
Fig. 2 **a** The growth rate of the phytoplankton r increases linearly in time at the rate v between $r(0) = r_0 > r_{min}$ and r_{max} (6). **b** The stable (red), unstable parts (blue) and folds $F_1(r)$, $F_2(r)$ (black lines) of the critical manifold S (11) organize the slow-fast motion in

phase space. Notice that S approximates the dynamics in the limit $\gamma \to 0$. Parameters of red trajectory: **a** $r(0) = r_0 = 0.4$, $v = 0.004$, **b**, **c** $P(0) = P_0 = e_P$, $Z(0) = Z_0 = e_Z$, $r(0) = r_0 = 0.4$, $v = 0.004$, $Rm = 0.4$, $\gamma = 0.05$. Other parameters see Table 1

conversion efficiency γ of the zooplankton which quantifies its turnover of phytoplankton biomass: the lower the turnover, the slower the zooplankton density changes in time. To emphasize that the change of the growth rate r is as slow as the development of zooplankton we make the ansatz, that $\eta = \gamma v$. Now we discuss the representation of the model taking this time scale separation into account. Following Truscott and Brindley (1994), we fix the conversion efficiency to $\gamma = 0.05$. Therefore, the phytoplankton population evolves on the fast time scale τ, while the zooplankton density and r change on the slow time scale t. Using the relationship between these two timescales $t = \gamma \tau$ we can write the extended dimensional TB-model (1)–(3) in slow time t:

$$\gamma \frac{dP}{dt} = rP\left(1 - \frac{P}{K}\right) - R_m Z \frac{P^2}{\alpha^2 + P^2} := f(P, Z, r), \qquad (4)$$

$$\frac{dZ}{dt} = R_m Z \frac{P^2}{\alpha^2 + P^2} - \kappa Z := g(P, Z), \qquad (5)$$

$$\frac{dr}{dt} = \begin{cases} v > 0 & \text{if } r_{min} < r < r_{max}, \\ 0 & \text{if } r = r_{min} \text{ or } r_{max} \end{cases} \qquad (6)$$

with $\kappa = \frac{\mu}{\gamma}$. From now on we will analyze (4), (5) and (6) and fix all parameters K, R_m, α, γ and μ according to Table 1, which is based on the original parameterization in Truscott and Brindley (1994) following the reasonable values formulated in (Uye 1986; Wake 1991). To allow for an easy comparison between our results and the results obtained by Truscott and Brindley (1994), we again employ the original formulation of the phytoplankton-zooplankton model (4)–(6) for the remainder of this work. Furthermore, we assume that

the phytoplankton and zooplankton populations coexist at low densities in a stable equilibrium at $t = 0$ before the growth rate of the phytoplankton r starts to increase linearly in time at the rate v.

Regular and quasi-static equilibria

When growth rate r is fixed, the autonomous TB-model (1)–(2) has three stationary solutions (equilibria). In addition to the extinction and the phytoplankton-only equilibria, both of which are unstable, there is a stable coexistence equilibrium in the (P, Z) phase plane (see Appendix A.2 for more details):

$$e(r) = \left(e_P, e_Z(r)\right) = \left(\sqrt{\frac{\mu \alpha^2}{\gamma R_m - \mu}}, \frac{r}{R_m}\left(1 - \frac{e_P}{K}\right)\left(\frac{\alpha^2 + e_P^2}{e_P}\right)\right). \qquad (7)$$

This equilibrium corresponds to the balance between the phytoplankton P and zooplankton Z populations, and is the starting point for our analysis of harmful algal blooms. It is always taken as the initial condition for the simulations. Most importantly, this equilibrium is linearly stable for the chosen parameter settings (Table 1) and all $r \in (r_{min}, r_{max})$. In other words, $e(r)$ never bifurcates in the classical autonomous model within the range of phytoplankton growth rates considered here.

The growth rate r changes over time, e.g., with increasing temperatures, and we need to consider the extended TB-model (4)–(6), where r becomes an additional dynamical variable. When $r = r_{max}$ or $r = r_{min}$, the long-term behavior of the TB-model is determined by the unique stable equilibrium $e(r = r_{max})$ or $e(r = r_{min})$, respectively. However, when $r \in (r_{min}, r_{max})$, the system has no equilibrium solutions

because $\frac{dr}{dt} = v > 0$. In this range, we will be interested in how the position of the state of stable coexistence $e(vt)$ changes with time, and how the system evolves relative to this changing $e(vt)$. Note that $e(vt)$ is referred to as a quasi-static equilibrium (Ashwin et al. 2012; Wieczorek et al. 2011), or a moving equilibrium (Vanselow et al. 2019; O'Keeffe and Wieczorek 2020; Wieczorek et al. 2021), which is computed by inserting $r = r(t) = vt$ into ((7)). The coexistence of the phytoplankton and zooplankton population at low densities is guaranteed when a solution stays near $e(vt)$ for small enough growth rates $v > 0$. In this case, the enhancing growth conditions of the phytoplankton are compensated by an increasing grazing pressure (increasing r causes an increase of $e_Z(r)$, Fig. 1a). However, an interesting instability occurs for larger rates of change v. In this case, the top-down control by the zooplankton relaxes since it is no longer able to balance the faster growing phytoplankton. This provokes an imbalance which results in a deviation of the solution of the extended TB-Model (1)–(3) from the quasi-static equilibrium $e(vt)$, manifesting in the formation of a phytoplankton bloom (Fig. 1b). This instability cannot be explained by the classical autonomous bifurcation theory, and requires an alternative approach. To fully understand this instability, we recall some basic concepts from the geometric singular perturbation theory for fast-slow systems.

The critical manifold

As shown in the previous Section, the system under investigation possesses a timescale separation. In fact, the dynamics of this 1-fast 2-slow system is slow for most of the time (Fig. 2b, single-headed arrows) with short time intervals of fast motion (double-headed arrows). Accordingly, it is reasonable to begin the study of our system by approximating the slow dynamics by taking $\gamma \to 0$. Note that we take $\gamma \to 0$ while keeping κ constant, which requires that $\mu \to 0$.

Taking the limit $\gamma \to 0$ for the slow time scale t gives the reduced model

$$0 = f(P, Z, r) \tag{8}$$

$$\frac{dZ}{dt} = g(P, Z) \tag{9}$$

$$\frac{dr}{dt} = \begin{cases} v > 0 & \text{if } r_{min} < r < r_{max}, \\ 0 & \text{if } r = r_{min} \text{ or } r_{max}, \end{cases} \tag{10}$$

for the evolution of the slow variables Z and r in slow time t on the so-called critical manifold S:

$$S = \left\{ (P, Z, r) \in \mathbb{R}^3 : rP\left(1 - \frac{P}{K}\right) \right. $$
$$\left. - R_m Z \frac{P^2}{\alpha^2 + P^2} = 0, P \geq 0, Z \geq 0, r_{min} \leq r \leq r_{max} \right\}, \tag{11}$$

in the (P, Z, r) phase space. Rearranging the condition above with respect to the Z-coordinate gives the cubic critical manifold formula

$$Z = h(P, r) = \frac{r}{R_m}\left(1 - \frac{P}{K}\right)\left(\frac{\alpha^2 + P^2}{P}\right), \tag{12}$$

Besides its approximation of the slow flow (one-headed arrow, Fig. 2b), the critical manifold S organizes the fast dynamics as follows: the (red) stable parts of S attract the fast flow, whereas the (blue) unstable part of S repels the fast flow. The stable and unstable parts connect at the two folds $F_1(r)$ and $F_2(r)$ (black lines) of S (see Appendix A.3 for the formulation of the folds). In the following, we display the critical manifold and the trajectories of the TB-model together in several figures. Notice that the critical manifold approximates the dynamics in the limit $\gamma = 0$, whereas the trajectories represent solutions of the TB-model for $0 < \gamma \ll 1$.

Rate-induced tipping triggers plankton bloom

If $v = 0.004$, the extended TB-model (4)–(6) in slow time t reveals a plankton bloom (Fig. 1b, red), but it does not if $v = 0.002$ (Fig. 1a, green). Since the difference in v is the only difference between the two setups (see Table 1 for the remaining parameters and the initial conditions), this indicates that, between the rates $v = 0.002$ and $v = 0.004$, the system crosses some quasithreshold that separates both dynamical regimes. To comprehend what creates the qualitative different behavior of the green and red trajectories (Fig. 1), we examine both trajectories in the (P, Z, r) phase space (Fig. 3). Since the stable (red), unstable parts (blue) and the folds (black solid lines) of the critical manifold organize the flow in phase space, we add the critical manifold S of the extended TB-model (4)–(6) to the phase portraits.

Starting at $e(vt)$ (7) at $t = 0$, the green trajectory ($v = 0.002$) reveals the expected behavior: it slowly follows the pathway of $e(vt)$ (gray dotted line, Fig. 3a) until it settles on the stable long-term state $e(r = r_{max})$. In this case, the slight increase in the zooplankton density, which implies an increasing grazing pressure, is sufficient to balance the growth of the phytoplankton. Consequently, we observe no plankton bloom. Since the green trajectory remains close to the quasi-static state $e(vt)$ (7) at all times, we say that the system *tracks* the stable quasi-static state $e(vt)$.

On the contrary, the red trajectory ($v = 0.004$) leaves the vicinity of the stable quasi-static state $e(vt)$ and performs a large excursion before converging to $e(r_{max})$ (Fig. 3b). At first, the red trajectory slowly proceeds towards the fold $F_1(r)$ (black solid line). In the vicinity of $F_1(r)$, its motion changes from slow to
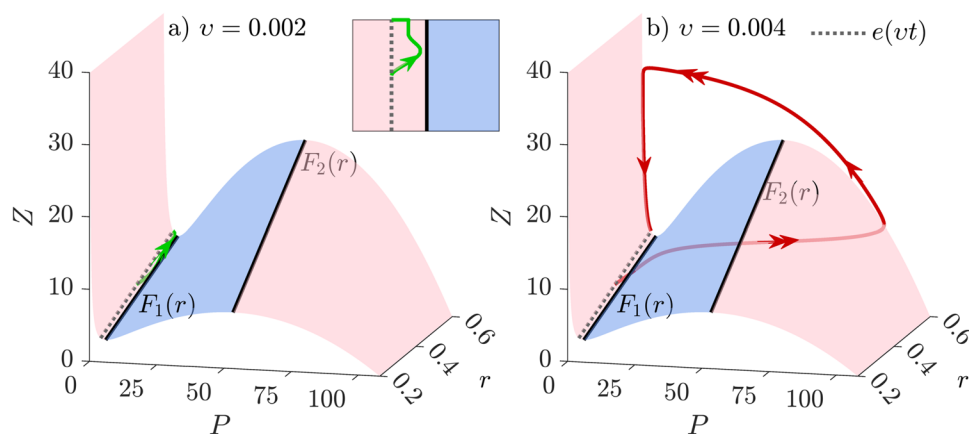
Fig. 3 Dynamics of the three-dimensional TB-model (4)–(6) for two different rates $v = 0.002$ and $v = 0.004$. Stable, unstable part and folds $F_1(r)$, $F_2(r)$ of the critical manifold S (11) are shown in red, blue and as 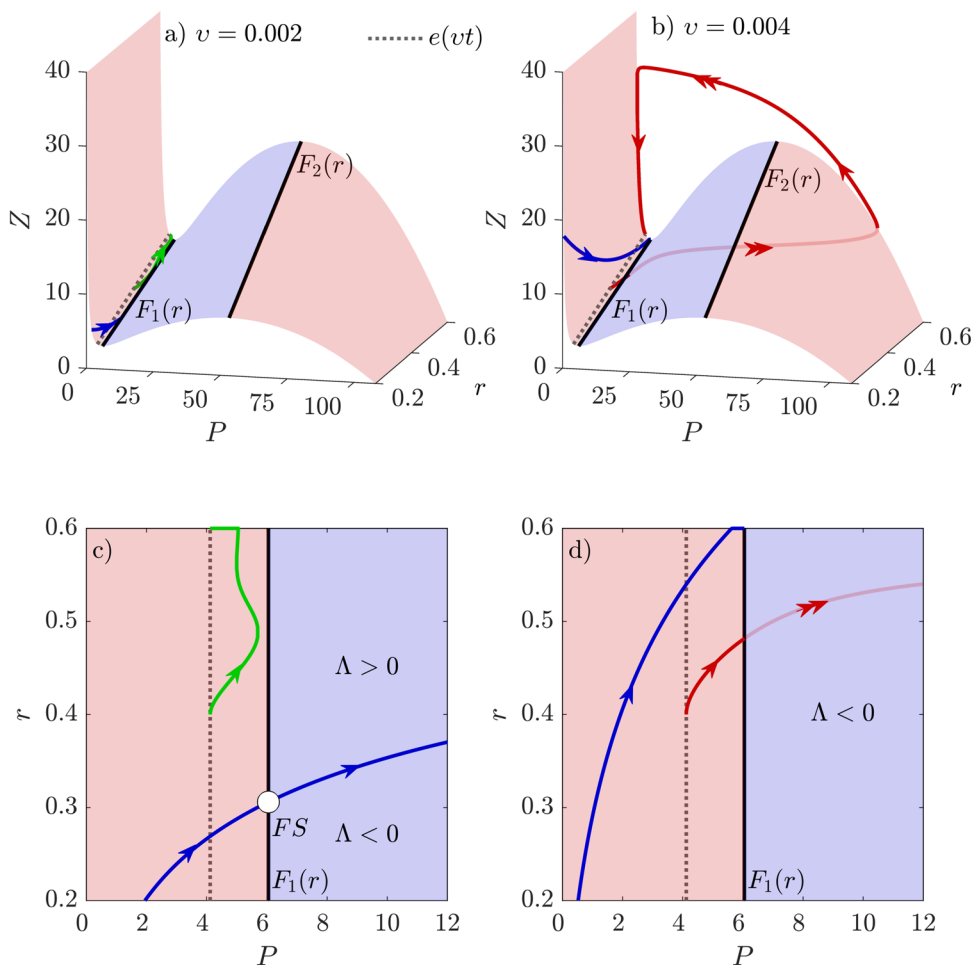solid black line. **a** The green trajectory remains close to the quasi-static equilibrium $e(vt)$ (7) (gray dotted line). **b** The red trajectory leaves the vicinity of $e(vt)$ close to the fold $F_1(r)$ towards the fast P-direction causing the formation of the plankton bloom. $P_0 = e_P$, $Z_0 = e_Z$ and $r_0 = 0.4$. Parameters see Table 1

fast and remains fast until it reaches the vicinity of the right stable part of S. This fast motion away from the quasi-static state $e(vt)$ entails a rapid increase in the phytoplankton density — the plankton bloom arises. When the trajectory reaches the vicinity of the right stable part of S, the plankton bloom possesses its maximal concentration. From here, the red trajectory slowly proceeds towards lower phytoplankton concentrations along the right stable part. Hence, the bloom slowly starts to recede due to an increasing zooplankton concentration controlling it. When the red trajectory approaches the second fold $F_2(r)$, it starts to move fast towards the left stable part: the bloom collapses rapidly due to the still persisting high zooplankton concentration. Along the left stable part, it finally converges to the stable long-term state $e(r_{max})$. Since the zooplankton feeds on the phytoplankton on a slower time scale than the phytoplankton reproduces, its evolution in time always lags behind the development of the phytoplankton. For instance, the zooplankton bloom reaches its peak when the phytoplankton density is close to zero (Figs. 1b and Fig. 3b).

Hence, in order to better understand the initiating mechanism, we examine the evolution of the fast variable P on the critical manifold S. To this end, we consider the *reduced system*, which describes the evolution of the slow variables Z and r on the critical manifold S. On the basis of the reduced system, we find a three-dimensional system that also captures the evolution of the fast variable P on S. Finally, for the sake of simplicity, we lower the complexity of the resulting system by *projecting* its three-dimensional flow on the two-dimensional critical manifold S using $Z = h(P, r)$ (see Appendix B for the transformation of the extended TB-model (4)–(6) to the projected-reduced system (13)–(14) and also for the detailed formulation of the numerator $\Lambda(P, r, v)$ and the denominator $\frac{\partial f^S(P,r)}{\partial P}\big|_S$ in Eq. (13)). The resulting projected-reduced system is given by:

$$\frac{\mathrm{d}P}{\mathrm{d}t} = -\frac{\Lambda(P, r, v)}{\frac{\partial f^S(P,r)}{\partial P}\big|_S}, \tag{13}$$

$$\frac{\mathrm{d}r}{\mathrm{d}t} = v. \tag{14}$$

Since the plankton bloom arises when the dynamics of the TB-model (4)–(6) changes from slow to fast motion close to the fold $F_1(r)$, we start our analysis of the projected-reduced system (13)–(14) on the stable part of S near the fold $F_1(r)$ and vary the phytoplankton growth rate r. Depending on the sign of the numerator $\Lambda(P_{F1}, r, v)$ which changes with r, we can distinguish three different types of trajectories (see Fig. 4 and Appendix B for more details): (i) For growth rates where $\Lambda(P_{F1}, r, v) < 0$, (red) trajectories are attracted to the fold $F_1(r)$. However, at the fold $F_1(r)$, the denominator $\frac{\partial f(P_{F1}^S, r, v)}{\partial P}\big|_S$ becomes zero. Hence, solutions of the projected-reduced system $P(t)$ blow up (go to infinity in finite time t) when they reach typical points on the fold $F_1(r)$. In other words, solutions cease to exist within S when they reach typical points on $F_1(r)$ (Fig. 4b, d). (ii) For values of r where $\Lambda(P_{F1}, r, v) > 0$, the (green) trajectories never reach $F_1(r)$ because they are repelled from the fold (Fig. 4a, c). (iii) There can be special points (special values of r) along the fold $F_1(r)$ at which both the numerator $\Lambda(P_{F1}, r, v) = 0$ and the denominator become zero such that $\frac{\mathrm{d}P}{\mathrm{d}t}$ remains finite (see Appendix B for more details). The corresponding (blue) trajectory approaches such a point on the fold $F_1(r)$ slowly and is able to cross it with finite speed (Fig. 4). Afterwards it proceeds slowly along the unstable part of S without being repelled in the fast P-direction (Fig 4c). Hence, this special trajectory — called *singular canard* — combines aspects of both dynamical regimes, i.e., of the green and red trajectory:

moving away from the quasi-static state (red, bloom) but
slowly (green, no bloom). The special fold point
$FS = (P_{FS}, r_{FS})$ (Fig. 4c), at which $\Lambda(P_{F1}, r, v) = 0$, is called
the *folded saddle singularity* (Szmolyan and Wechselberger
2001) (see Appendix B for the computation of the folded
saddle and the canard). Since the term $\Lambda(P_{F1}, r, v)$ depends
on the rate v, the position of the folded saddle and thus the
position of the singular canard on the critical manifold S also
depends on the rate v (see Appendix B). For this reason, the
location of the singular canard changes from the scenario
without bloom ($v = 0.002$, green trajectory) to the scenario
with plankton bloom ($v = 0.004$, red trajectory). For
$v = 0.002$, the singular canard is located below the initial
condition of the green trajectory. Fold points above the sin-
gular canard, respectively above the folded saddle FS
($P_F > P_{FS}$ and $r_F > r_{FS}$), are repelling fold points ($\Lambda > 0$,
Fig. 4c). Consequently, the green trajectory is repelled by
the part of the fold $F_1(r)$ above the singular canard and tracks
the stable quasi-static state $e(vt)$: no bloom is formed. For
$v = 0.004$, the singular canard is located at higher values of
the growth rate r. As a consequence, the singular canard is
now located above the initial condition of the red trajectory.

The fold points below the singular canard are attracting
($\Lambda < 0$) and therefore, the red trajectory crosses the fold and
runs away in the fast direction. As a result, a plankton bloom
emerges ($\Lambda < 0$, Fig. 4d). Thus, in the limit $\gamma \to 0$, there
exists an isolated *critical rate* $v = v_{crit}$ for each initial condi-
tion. This critical rate is the value of v for which the given
initial condition lies exactly on the v-dependent singular
canard. This singular canard can be thought of as a *singular
threshold* for rate-induced tipping.

The critical manifold S only approximates the slow dynam-
ics in the limit when the time scale separation is perfect,
i.e., $\gamma = 0$ (Wechselberger et al. 2013). However, in the full
extended TB-model (4)–(6), we consider a finite time scale
separation between phytoplankton and zooplankton, and,
hence, $0 < \gamma \ll 1$. To evaluate if the singular canard persists
in the full extended TB-model (neither reduced nor projected),
we need to translate the dynamics in the singular limit ($\gamma = 0$)
to the full dynamics ($0 < \gamma \ll 1$). In the full system, the criti-
cal manifold S is replaced with a nearby slow manifold S_γ, and
the stable and unstable parts of S_γ typically split along the fold
(Fig. 5b). They only intersect near the point FS (white circle
in Fig. 5a) which represents the folded saddle in the singular

limit system. This intersection point gives rise to a *maximal canard* that crosses from the stable part of the slow manifold into the unstable part of the slow manifold where it stays for as long as the unstable part exists (Fig. 5b). On the lower-*r* side of the maximal canard, the unstable part is located above the stable part. Hence, (red) trajectories can proceed beneath the unstable part and then run away in the fast direction — a bloom arises. Conversely, on the higher-*r* side of the maximal canard, the unstable part is located below the stable part whereby (green) trajectories proceed above the unstable part and are thus repelled back towards the left stable part — *P* and *Z* remain at low densities.

Therefore, also in the full system ($0 < \gamma \ll 1$), there is a boundary separating (green) trajectories, reflecting the maintenance of the balance between *P* and *Z*, from (red) trajectories, that show the formation of a plankton bloom. The difference is that, in contrast to the singular case ($\gamma = 0$), this boundary is not clear cut. This can be understood as follows. In addition to the maximal canard, which is in a one-to-one correspondence with the singular canard (Wechselberger et al. 2013) and follows the unstable part of the slow manifold for the longest time, there are additional canards. These additional canards stay close to the maximal canard for some shorter time, after which they leave the unstable part of the slow manifold towards the left stable part. This whole family of canards is responsible for the transition to a plankton bloom, and is referred to as a *quasithreshold* for rate-induced tipping (Wieczorek et al. 2021; O'Sullivan et al. 2022). Crossing such a quasithreshold occurs for a narrow *critical range* of υ rather than at one isolated critical rate $\upsilon = \upsilon_{crit}$.

In summary, we have demonstrated that the harmful algal bloom or red tide is solely triggered by rate-induced tipping (Ashwin et al. 2012; Wieczorek et al. 2011). An increase

of the rate of change υ, which describes the speed at which the growth rate of the phytoplankton *r* increases, changes the position of the maximal canard on the slow manifold S_γ in a way that causes the (red) trajectory to leave the region nearby $e(\upsilon t)$, resulting in the formation of a plankton bloom in the full system (Fig. 4b).

R-tipping can trigger two sequentially occurring plankton blooms

Interestingly, the extended TB-model (4)–(6) can show more than one plankton bloom (Fig. 6). In the previous section, we have demonstrated that if initial conditions of the extended TB-model (4)–(6) are located on S_γ on the lower-*r* side of the maximal canard, the model shows a rate-induced plankton bloom. Clearly, when the red trajectory still finds itself on the lower-*r* side of the maximal canard following the bloom, it can exhibit another bloom before it settles on the long-term state $e(r_{max})$ (Fig. 6). The number of possibly recurring blooms naturally increases with parameter changes that shift the maximal canard towards higher values of *r* accompanying a higher maximum growth rate r_{max}. For instance, increasing the maximum growth rate r_{max} from 0.6 to 0.8 and simultaneously increasing the rate of change υ to 0.006 triggers two recurring plankton blooms (Fig. 6). Other parameter changes that promote the occurrence of multiple blooms are an increase of the zooplankton's mortality ω or a decrease of the zooplankton's attack rate R_m (see Appendix C for more details). Obviously, parameter changes reducing the grazing pressure and therefore relaxing the top-down control by the zooplankton encourage the formation of more than one bloom.
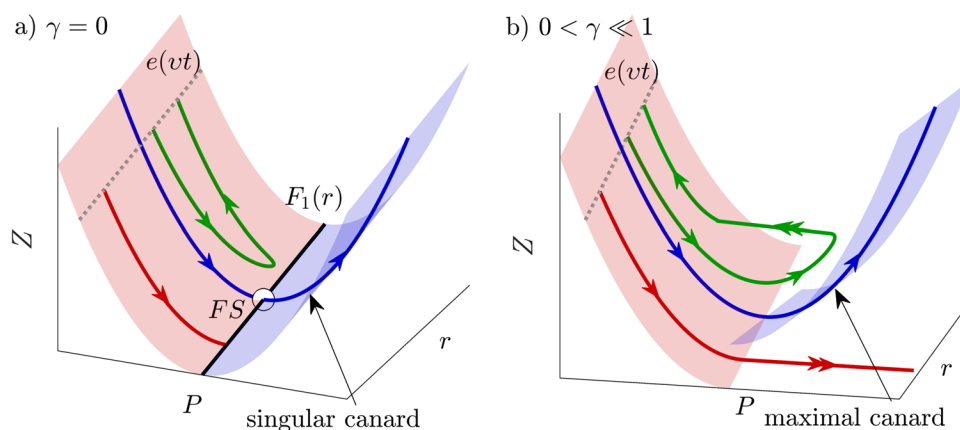

Fig. 5 a Stable (red) and unstable (blue) part of the critical manifold *S* merge along the fold $F_1(r)$ (black solid line). (Red) trajectories cease to exist at the fold whereas a singular canard (blue trajectory) is able to cross the fold via the point *FS*. (Green) trajectories are repelled by the fold and approach $e(\upsilon t)$ (gray dashed line). **b** Stable and unstable part are perturbed along the position of the fold $F_1(r)$ for $\gamma = 0$. At their intersection point (*FS* when $\gamma \to 0$), the maximal canard crosses from stable to unstable part separating (green) trajectories that are repelled by the unstable part from (red) trajectories that leave the stable part in the fast *P*-direction

Fig. 6 Two sequentially recurring plankton blooms occur if the red trajectory reaches the left stable part of the critical manifold S (red) beneath the canard (blue) after performing the first excursion. Parameter: $P_0 = e_P$, $Z_0 = e_Z$, $r_0 = 0.4$, $r_{max} = 0.8$. Other parameters see Table 1
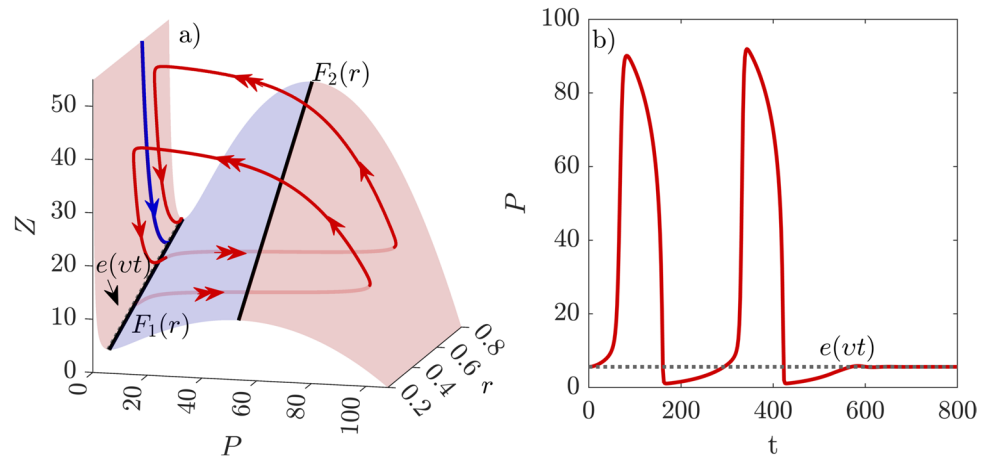
Discussion

In ecology, several factors which are responsible for the emergence of regularly and irregularly occurring plankton blooms have already been identified (Behrenfeld 2014; Sommer et al. 2012; Lewandowska et al. 2015; Freund et al. 2006; Chakraborty and Feudel 2014) but still, some mechanisms are not fully understood. Hence, there exists some uncertainty how future climate change will impact the severity and frequency of plankton blooms (Doney 2006; Hillebrand et al. 2018; Winder et al. 2012). We demonstrate that rate-induced tipping constitutes a possible mechanism explaining the occurrence of erratically occurring blooms such as red tides. We proceed from the work of Truscott and Brindley (1994) in which they developed a time-scaled phytoplankton (P, fast variable)-zooplankton(Z, slow variable) model using ideas from the theory of excitable media. In their work, they studied the response of the model to fast environmental changes that provoke an increase of the phytoplankton's growth rate. Depending on its speed of change, the model reveals two disparate behaviors: conservation of the balance of P and Z (no bloom), or an imbalance of both that manifests in a plankton bloom. Using fast-slow system theory, we uncover the quasithreshold phenomenon which separates both behaviors in state space: a special trajectory called maximal canard together with a family of shorter canards. The position of the quasithreshold determines whether solutions remain close to the balance state corresponding to low plankton concentrations or leave its vicinity leading to an imbalance that manifests in a large plankton bloom. Since the location of the quasithreshold depends on the speed, or the rate, at which the phytoplankton growth rate increases, rate-induced tipping constitutes the mechanism being responsible for the emergence of the harmful algal bloom. We further demonstrate that decreasing the grazing pressure or broadening the interval in which the growth rate increases allows for multiple recurring plankton blooms.

In accordance with Truscott and Brindley (1994), we assume that the rate-induced HAB is triggered by fast enhancing growth conditions of the phytoplankton due to temperatures increasing at a certain speed. However, other scenarios in which the growth conditions improve gradually at a certain speed are just as conceivable, e.g., due to an increase of the light intensity (Rumyantseva et al. 2019; Winder et al. 2012) or the nutrient supply (Largier 2020; Guseva and Feudel 2020). Moreover, an imbalance between phytoplankton growth and predator control can be obtained if traits of the grazers, such as attack rate or mortality rate, are affected by rapid environmental changes (Behrenfeld 2010; Busch et al. 2019). Consequently, the notion that rate-induced tipping is able to cause irregularly occurring plankton blooms does not depend on any particular environmental driver but rather on its dynamics: As long as any environmental condition changes at a certain speed, rate-induced tipping is a potential trigger mechanism of plankton blooms. The same argument holds also for regular spring blooms as long as their grazing function is described with the same functional response as for harmful algal species.

A second precondition for the occurrence of rate-induced blooms is that phytoplankton reproduces faster than their grazers. This condition is often met since the hourly to daily cell division of phytoplankton (Franks 2001) is typically much faster than the reproduction of their grazers which mainly possess generation times from hours to a month (Hirsche 2013; Klais et al. 2016). Empirical evidence for the importance of time scale separation in the formation of plankton blooms comes from iron enrichment experiments carried out in the 1990s (Cavender-Bares et al. 1999; Cullen 1995; Morel et al. 1991). A particularly vivid example was given by the IronEx II experiment (Coale et al. 1996), in which iron enrichment only led to about a doubling of the picoplankton biomass, but up to an 85-fold increase in some diatom species (phytoplankton). Picoplankton are usually grazed by protists which have often short response time

scales — similar to the generation times of the picoplankton. Accordingly, protists can keep the picoplankton at low densities. On the contrary, phytoplankton like diatoms tend to be grazed by metazoan zooplankton, which have relatively long generation times and therefore long response times which allows for the formation of temporary imbalances and thus for the formation of plankton blooms (Franks 2001).

Finally, we want to point out two shortcomings of the current state of the art in ecological modeling concerning the impact of environmental change. We have seen that the observation of rate-induced phenomena, like the formation of plankton blooms, depends on (i) the evolution of the time horizon of environmental change and (ii) the presence of multiple time scales in species' development. (i) Regarding the time scale of environmental change, most studies employ the concept called "tipping point" which underlies the idea of a catastrophic bifurcation of the involved long-term states if a critical threshold is exceeded (Scheffer et al. 2001; Lenton et al. 2008; Lenton 2020; Krönke et al. 2020; Dakos et al. 2019). Bifurcation analysis implies that environmental conditions change infinitely slow. Hence, tipping points are only relevant in cases where it can be assumed that the speed of environmental change is much slower than the intrinsic ecological dynamics. By contrast, rate-induced tipping occurs on time scales comparable to the dynamics of ecosystems and, hence becomes apparent only in the transient dynamics — the dynamics prior to the long-term dynamics (Hastings et al. 2018; Morozov et al. 2020). Hence, the plankton bloom described in this work would be overlooked if we would focus exclusively on the long-term dynamics.

Concerning the omission of the presence of multiple time scales: if the presence of multiple time scales is neglected, no canard solution can exist and thus, without the existence of any other instability (e.g., a tipping point), no rate-induced phenomena can be observed in the system. Such phenomena are, however, crucial when examining the effect of the speed of environmental change as they reveal critical states which would be missed otherwise. Since present climate change accelerates environmental changes, corresponding studies will be of paramount importance in the future (Walther et al. 2002; Parmesan 2006; Smith et al. 2015).

In summary, to meet the accelerating speed of environmental change, we suggest three key elements for consideration in future ecological studies. First of all, we believe that it will be of paramount importance to take into account the temporal evolution of environmental disturbances or changes (which is usually not infinitely slow). Secondly, in order to capture the full impact of fast rates of environmental change, it is essential to explicitly consider the different intrinsic time scales which are present in an ecological system. Thirdly, since critical phenomena — like rate-induced tipping — act on time scales comparable to the system dynamics, the evaluation of environmental impacts should not be exclusively based on the long-term response but on the transient dynamics as well. In addition we would like to

emphasize that an experimental test for rate-induced transitions in the laboratory requires explicit measurement of the rate of environmental change.

For certain, the Truscott-Brindley model misses essential physical processes, such as vertical mixing and sinking, as well as other ecological processes, such as viral infection and the diverse composition of interacting communities. However, just like any theoretical model, due to its delightful simplicity it enables the understanding of otherwise unsolvable relationships between ecological actors and their environment. Our findings suggest that plankton communities, which typically involve species evolving on multiple time scales, are potentially prone to environmental disturbances evolving at a certain speed. Hence, we propose to consider multiple time scales in theoretical models of ecosystems, such as food webs, and to examine their transient dynamics.

Appendix A. The Truscott-Brindley model

A.1 Non-dimensionalization

The phytoplankton(P)-zooplankton(Z) model developed by Truscott and Brindley (1994) is given by the following two equations:

$$\frac{dP}{d\tau} = rP\left(1 - \frac{P}{K}\right) - R_m Z \frac{P^2}{\alpha^2 + P^2}, \tag{A1}$$

$$\frac{dZ}{d\tau} = \gamma R_m Z \frac{P^2}{\alpha^2 + P^2} - \mu Z, \tag{A2}$$

with the growth rate of the phytoplankton population r and its carrying capacity K. The attack rate of the zooplankton R_m, its half-saturation constant α, conversion efficiency γ and mortality rate μ complete the model.

In the following, we introduce the non-dimensional variables $\hat{P} = \frac{P}{K}$, $\hat{Z} = \frac{Z}{K}$ and the non-dimensional time $\hat{t} = \tau \cdot R_m$. Replacing P, Z and τ by their non-dimensional equivalent, we can rewrite the TB-model (A1)–(A2) as follows:

$$\frac{d\hat{P}}{d\hat{t}} = \frac{r}{R_m}\hat{P}(1 - \hat{P}) - \hat{Z}\frac{\hat{P}^2}{\left(\frac{\alpha}{K}\right)^2 + \hat{P}^2}, \tag{A3}$$

$$\frac{d\hat{Z}}{d\hat{t}} = \gamma\hat{Z}\left(\frac{\hat{P}^2}{\left(\frac{\alpha}{K}\right)^2 + \hat{P}^2} - \frac{\mu}{\gamma R_m}\right). \tag{A4}$$

Setting $\delta = \frac{\alpha}{K}$, $\beta = \frac{r}{R_m}$ and $\omega = \frac{\mu}{\gamma R_m}$, the non-dimensional TB-model (A3)–(A4) becomes:

$$\frac{\mathrm{d}\hat{P}}{\mathrm{d}\hat{t}} = \beta\hat{P}(1-\hat{P}) - \hat{Z}\frac{\hat{P}^2}{\delta^2 + \hat{P}^2}, \tag{A5}$$

$$\frac{\mathrm{d}\hat{Z}}{\mathrm{d}\hat{t}} = \gamma\hat{Z}\left(\frac{\hat{P}^2}{\delta^2 + \hat{P}^2} - \omega\right). \tag{A6}$$

The parameter γ quantifies the separation between the time scale of the phytoplankton and the time scale of the zooplankton. For this reason, we call γ the time scale parameter. If $\gamma < 1$, the zooplankton population reproduces slower than the phytoplankton and vice versa. For $\gamma = 1$, there exists no time scale separation.

We further assume that the growth rate of the phytoplankton r becomes time-dependent: $r = r(\tau)$ and increases at a constant rate η:

$$\frac{\mathrm{d}r}{\mathrm{d}\tau} = \eta. \tag{A7}$$

Using the dimensionless time $\hat{t} = \tau \cdot R_m$, Eq. (A7) becomes:

$$\frac{\mathrm{d}r}{\mathrm{d}\hat{t}/R_m} = \eta, \tag{A8}$$

with $\beta = \frac{r}{R_m}$, we can write:

$$\frac{\mathrm{d}\beta}{\mathrm{d}\hat{t}} = \eta. \tag{A9}$$

Equations (A5), (A6) and (A9) show the three-dimensional plankton model in fast time $\hat{t}$. We now assume that the temporal evolution of r and β happens on the same time scale as the temporal evolution of zooplankton. Therefore we use the time scale separation parameter to scale the rate of change of r: $\eta = \gamma \upsilon$. We can write the whole model system in slow time $\tilde{t} = \gamma\hat{t}$ using $\frac{\mathrm{d}}{\mathrm{d}\hat{t}} = \frac{\mathrm{d}}{\mathrm{d}\tilde{t}}\frac{\mathrm{d}\tilde{t}}{\mathrm{d}\hat{t}} = \frac{\mathrm{d}}{\mathrm{d}\tilde{t}}\gamma$:

$$\gamma\frac{\mathrm{d}\hat{P}}{\mathrm{d}\tilde{t}} = \beta\hat{P}(1-\hat{P}) - \hat{Z}\frac{\hat{P}^2}{\delta^2 + \hat{P}^2}, \tag{A10}$$

$$\frac{\mathrm{d}\hat{Z}}{\mathrm{d}\tilde{t}} = \hat{Z}\left(\frac{\hat{P}^2}{\delta^2 + \hat{P}^2} - \omega\right), \tag{A11}$$

$$\frac{\mathrm{d}\beta}{\mathrm{d}\tilde{t}} = \upsilon \tag{A12}$$

A.2 Long-term states and linear stability

To find the long-term states of the TB-model (A1)–(A2), we set the dynamics of the phytoplankton and zooplankton population equal to zero:

$$0 = rP\left(1 - \frac{P}{K}\right) - R_m Z\frac{P^2}{\alpha^2 + P^2}, \tag{A13}$$

$$0 = \gamma R_m Z\frac{P^2}{\alpha^2 + P^2} - \mu Z. \tag{A14}$$

Solving Eqs. (A13)–(A14) with respect to P and Z leads to the following three long-term states e_1–$e_3(r)$ (A15)–(A17)

$$e_1 = (e_P, e_Z) = (0, 0), \tag{A15}$$

$$e_2 = (e_P, e_Z) = (K, 0), \tag{A16}$$

$$e_3(r) = (e_P, e_Z(r)) = \left(\sqrt{\frac{\mu\alpha^2}{\gamma R_m - \mu}}, \frac{r}{R_m}\left(1 - \frac{e_P}{K}\right)\left(\frac{\alpha^2 + e_P^2}{e_P}\right)\right). \tag{A17}$$

The equilibrium e_1 describes the situation in which phytoplankton and zooplankton are extinct. In e_2, the phytoplankton possesses the maximum density that the environment can "carry" (K) while the zooplankton is extinct. In the third equilibrium $e_3(r)$, phytoplankton and zooplankton coexist at densities unequal zero. Notice that only the equilibrium $e_3(r)$ depends on the growth rate of the phytoplankton r. Within the interval $r \in [0.2\ 2]$, it represents the unique stable state of the TB-model (Fig. 7). Hence for values of the growth rate between r_{min} and r_{max}, the phytoplankton and zooplankton coexist in a stable long-term equilibrium when $t \to \infty$.

A.3 The critical manifold

The extended Truscott-Brindley model with time-dependent growth rate r can be written in slow time $t = \gamma\tau$ ($\kappa = \mu/\gamma$, $\upsilon = \eta/\gamma$) (Truscott and Brindley 1994):

$$\gamma\frac{\mathrm{d}P}{\mathrm{d}t} = rP\left(1 - \frac{P}{K}\right) - R_m Z\frac{P^2}{\alpha^2 + P^2} := f(P, Z, r), \tag{A18}$$

$$\frac{\mathrm{d}Z}{\mathrm{d}t} = R_m Z\frac{P^2}{\alpha^2 + P^2} - \kappa Z := g(P, Z), \tag{A19}$$

$$\frac{\mathrm{d}r}{\mathrm{d}t} = \begin{cases} \upsilon > 0 & \text{if } r_{min} < r < r_{max}, \\ 0 & \text{if } r = r_{min} \text{ or } r_{max}. \end{cases} \tag{A20}$$

The TB-model with time-dependent growth rate r (A18)–(A20) is determined, as the original TB-model, by a fast and a slow time scale. In fact, the dynamics of such slow-fast systems is primarily slow with short interruption by fast motion. The critical manifold S approximates the slow motion and is therefore a useful tool to obtain a first impression of a part of the full dynamics.

Fig. 7 Linear stability of the three equilibria e_1–$e_3(r)$ (A15)–(A17) of the TB-model (A1)–(A2) depending on the growth rate $r \in [0.2 \; 2]$. Solid/dotted line denotes the real parts of the eigenvalues $\lambda_{1,2} < 0$ (stable) respectively $\lambda_{1,2} > 0$ (unstable). For the other parameters see Table 1
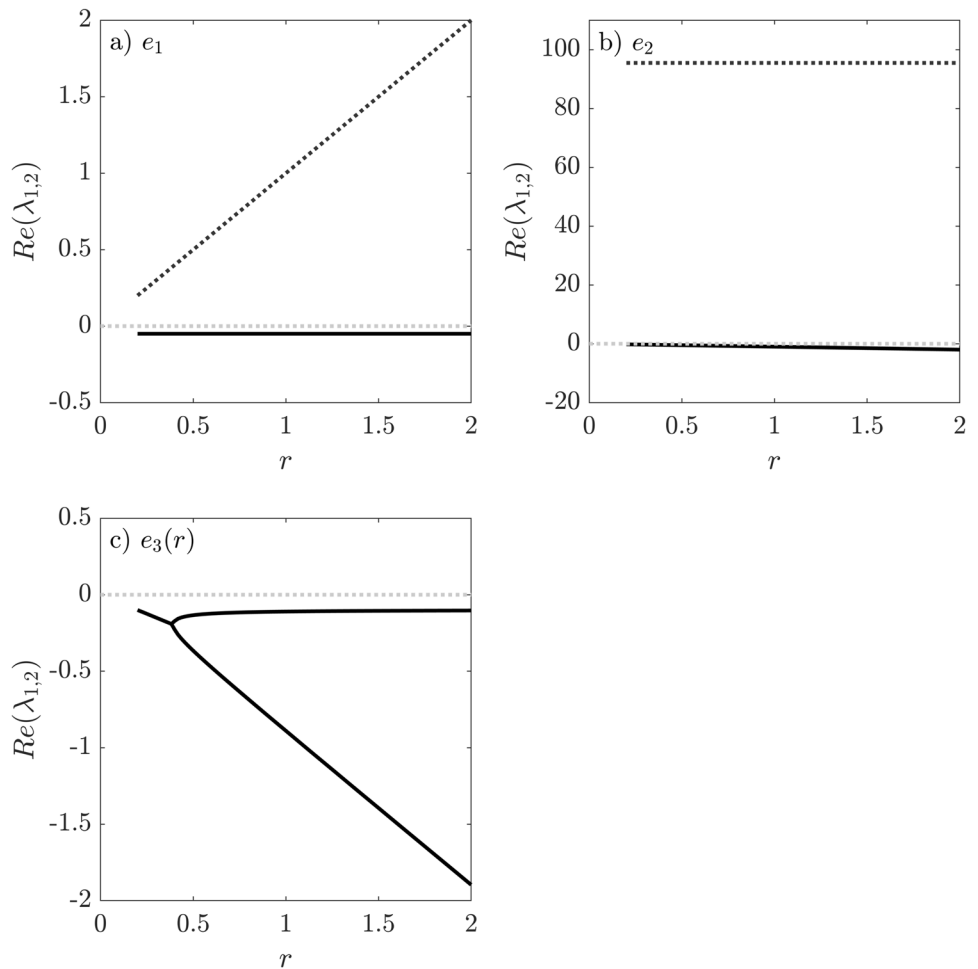
$$S = \left\{ (P, Z, r) \in \mathbb{R}^3 \; : \; rP\left(1 - \frac{P}{K}\right) \right.$$
$$\left. - R_m Z \frac{P^2}{\alpha^2 + P^2} = 0, P \geq 0, Z \geq 0, r_{min} \leq r \leq r_{max} \right\},$$
$$(A21)$$

The critical manifold S (A21) can be further written as:

$$Z = h(P, r) = \frac{r}{R_m}\left(1 - \frac{P}{K}\right)\left(\frac{\alpha^2 + P^2}{P}\right), \qquad (A22)$$

with the two folds $F_{1,2}(r) = (P_{F_{1,2}}, Z_{F_{1,2}})$ given by the following equations

$$\frac{2P_{F_{1,2}}^3}{K} - P_{F_{1,2}}^2 + \alpha = 0, \qquad (A23)$$

$$Z = \frac{r}{R_m}\left(1 - \frac{P_{F_{1,2}}}{K}\right)\left(\frac{\alpha^2 + P_{F_{1,2}}^2}{P_{F_{1,2}}}\right). \qquad (A24)$$

Appendix B. The canard trajectory

When studying the slow-fast dynamics of the extended TB-model (B25)–(B27) with time-dependent growth rate r for different rates v, we find a plankton bloom when the growth rate r increases faster than $v \approx 0.003$ ($\eta \approx 0.0015$) (Fig. 1, see Sec. "Rate-induced tipping triggers plankton bloom" for more details)

$$\gamma \frac{dP}{dt} = rP\left(1 - \frac{P}{K}\right) - R_m Z \frac{P^2}{\alpha^2 + P^2} := f(P, Z, r) \qquad (B25)$$

$$\frac{dZ}{dt} = R_m Z \frac{P^2}{\alpha^2 + P^2} - \kappa Z := g(P, Z) \qquad (B26)$$

$$\frac{dr}{dt} = v > 0. \qquad (B27)$$

To simplify notations, we use from now on the following abbreviations. Note that q is denoting f and g and k stands for P, Z and r.

$$q^S(P,r) = q(P,Z,r)\big|_{Z=h(P,r)}, \tag{B28}$$

$$q_k^S(P,r) = \frac{\partial q(P,Z,r)}{\partial k}\bigg|_{Z=h(P,r)}. \tag{B29}$$

The bloom forms when (red) trajectories cross the fold $F_1(r)$ of the critical manifold S and run away in the fast P-direction (Fig. 4). For this reason, we study the fast flow close to the fold $F_1(r)$ on the critical manifold S. To study the dynamics on S, we set the fast dynamics $\frac{dP}{dt}$ equal to zero ($\gamma \to 0$) which gives the *reduced system*:

$$0 = f(P,Z,r), \tag{B30}$$

$$\frac{dZ}{dt} = g(P,Z), \tag{B31}$$

$$\frac{dr}{dt} = v > 0. \tag{B32}$$

Differentiating the algebraic constraint (B30) with respect to the slow time t leads to:

$$0 = \frac{d}{dt}f(P,Z,r), \tag{B33}$$

$$0 = f_P(P,Z,r) \cdot \frac{dP}{dt} + f_Z(P,Z,r)\, g(P,Z) + f_r(P,Z,r)v, \tag{B34}$$

$$\frac{dP}{dt} = -\frac{f_Z(P,Z,r)\, g(P,Z) + f_r(P,Z,r)v}{f_P(P,Z,r)}. \tag{B35}$$

The Eq. (B35) describes the fast flow P on the critical manifold S. Replacing the constrain Eq. (B30) by Eq. (B35), we obtain:

$$\frac{dP}{dt} = -\frac{f_Z(P,Z,r)\, g(P,Z) + f_r(P,Z,r)v}{f_P(P,Z,r)}, \tag{B36}$$

$$\frac{dZ}{dt} = g(P,Z), \tag{B37}$$

$$\frac{dr}{dt} = v > 0. \tag{B38}$$

Using $Z = h(P,r)$ (A22), we *project* the flow onto the critical manifold S. The so-called *projected-reduced system* is given by:

$$\frac{dP}{dt} = -\frac{f_Z^S(P,r)\, g^S(P) + f_r^S(P,r)v}{f_P^S(P,r)}, \tag{B39}$$

$$\frac{dr}{dt} = v > 0. \tag{B40}$$

With $\Lambda(P,r,v) = f_Z^S(P,r)\, g^S(P) + f_r^S(P,r)v$ and $f_P^S(P,r) = f\frac{\partial f(P,r)}{\partial P}\big|_S$ we can write the projected-reduced system as:

$$\frac{dP}{dt} = -\frac{\Lambda(P,r,v)}{\frac{\partial f(P,r)}{\partial P}\big|_S}, \tag{B41}$$

$$\frac{dr}{dt} = v > 0. \tag{B42}$$

For completeness, we write the projected-reduced system in full terms

$$\frac{dP}{dt} = \frac{\frac{-\gamma r R_m P^3\left(1-\frac{P}{K}\right)}{\alpha^2+P^2} + \kappa rP\left(1 - \frac{P}{K}\right) + \left(P - \frac{P^2}{K}\right)v}{\left(-r + \frac{2rP}{K} + \frac{2\alpha^2 r\left(1-\frac{P}{K}\right)}{\alpha^2+P^2}\right)} \tag{B43}$$

$$\frac{dr}{dt} = v > 0. \tag{B44}$$

If $f_P^S(P,r) = 0$ (B39), the flow on the critical manifold S (11) is not defined — it goes to infinity in finite time. Unfortunately, these points for which $f_P^S(P,r) = 0$ are the fold points of the critical manifold S (11). Since the bloom formation occurs close to the fold, we have to enable the analysis near the fold $F_1(r)$. This can be achieved by using the scaling known as *desingularization*:

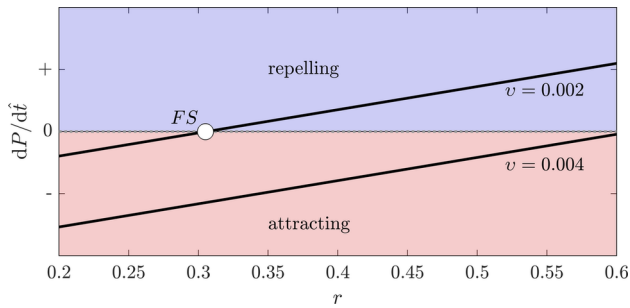$$t = -\hat{t} \cdot f_P^S(P,r), \tag{B45}$$

which preserves the direction of time on the stable part of the critical manifold S (red, Fig. 9), but reverses it on the unstable part (blue, Fig. 9). The desingularized system is given by:

$$\frac{dP}{d\hat{t}} = f_Z^S(P,r)\, g^S(P) + f_r^S(P,r)v, \tag{B46}$$

$$\frac{dr}{d\hat{t}} = -f_P^S(P,r)v, \tag{B47}$$

respectively in full terms,

$$\frac{dP}{d\hat{t}} = \frac{-\gamma r R_m P^3\left(1 - \frac{P}{K}\right)}{\alpha^2 + P^2} + \kappa rP\left(1 - \frac{P}{K}\right) + \left(P - \frac{P^2}{K}\right)v, \tag{B48}$$

$$\frac{\mathrm{d}r}{\mathrm{d}\hat{t}} = \left(-1 + \frac{2P}{K} + \frac{2\alpha^2\left(1 - \frac{P}{K}\right)}{\alpha^2 + P^2}\right)v. \tag{B49}$$

Interestingly, setting $\frac{\mathrm{d}r}{\mathrm{d}\hat{t}} = 0$:

$$0 = \left(-1 + \frac{2P}{K} + \frac{2\alpha^2\left(1 - \frac{P}{K}\right)}{\alpha^2 + P^2}\right), \tag{B50}$$

Fig. 8 The fast flow $\frac{\mathrm{d}P}{\mathrm{d}\hat{t}}$ (B48) (black solid line) on the fold $F_1(r)$ (A23)–(A24) is shown for two different rates $v = 0.002$ and $v = 0.004$. Fold Points with $\frac{\mathrm{d}P}{\mathrm{d}\hat{t}} < 0$ attract trajectories (red) while fold points with $\frac{\mathrm{d}P}{\mathrm{d}\hat{t}} > 0$ are repelling (blue). The fast flow $\frac{\mathrm{d}P}{\mathrm{d}\hat{t}}$ remains only finite at the point FS. For other parameters see Table 1

and rearranging Eq. (B50) with respect to P gives the P_{F_1}-values of the fold $F_1(r)$. When we further set P_{F_1} into Eq. (B48), we can analyze the fast flow $\frac{\mathrm{d}P}{\mathrm{d}\hat{t}}$ at the fold $F_1(r)$ (Fig. 8). For $v = 0.002$, there exist a special solution at which $\frac{\mathrm{d}P}{\mathrm{d}\hat{t}} = 0$

Fig. 9 Dynamics of the desingularized system (B48)–(B49) for two different rates $v = 0.002$ (**a**, **c**, **e**) and $v = 0.004$ (**b**, **d**, **f**). The singular canard (blue trajectory) is given by the stable manifolds of the folded saddle FS (white filled circle). It represents the threshold separating (green) tracking from (red) tipping trajectories. **a**, **c** The green trajectory starts above the singular canard and tracks — no bloom emerges (**e**). **b**, **d** The red trajectory starts below the canard, is attracted by the fold $F_1(p, r)$, crosses it and approaches the stable folded focus FF (black filled circle) — a plankton bloom occurs (**f**)
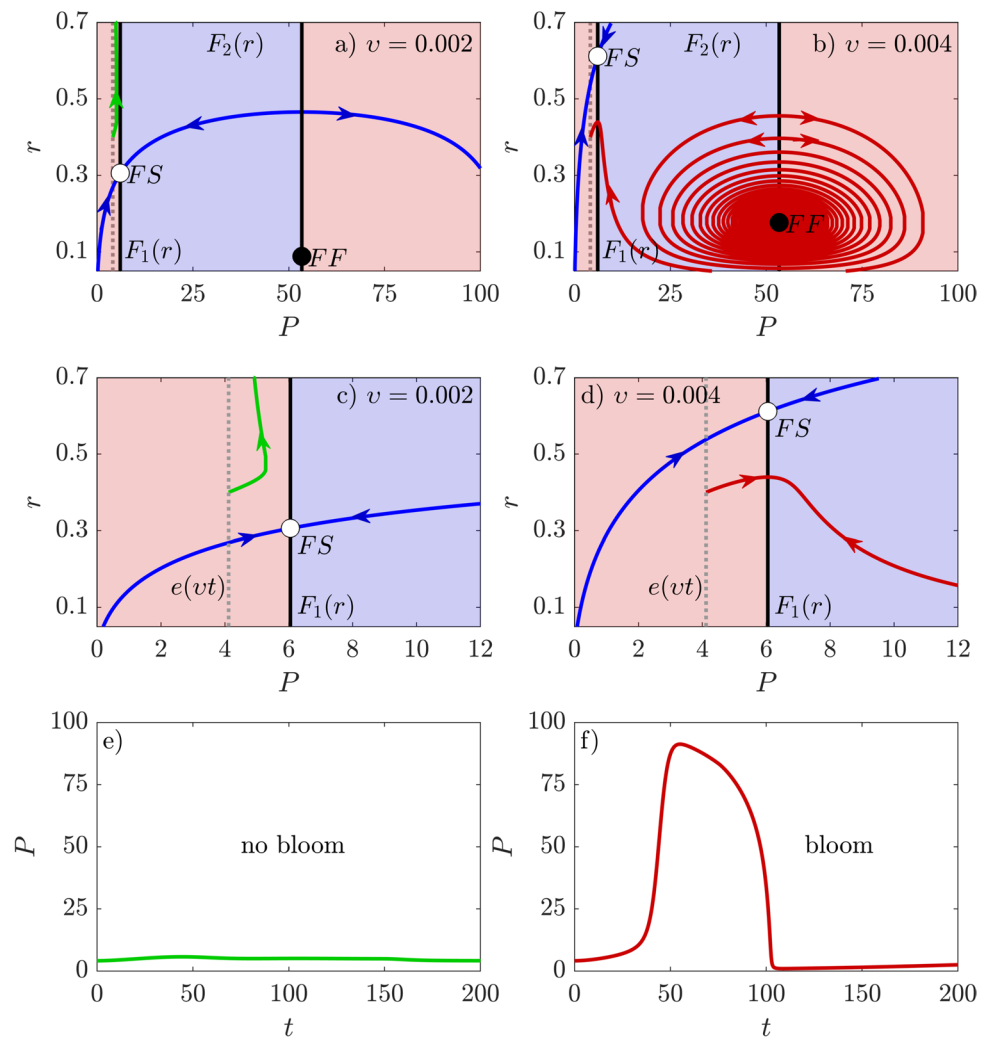
(white circle) within $r \in [0.2 \ 0.6]$. This special solution is an equilibrium of the desingularized system (B48)–(B49) and it marks the boundary between fold points that attract trajectories ($\frac{dP}{d\hat{t}} < 0$, red) and fold points that repel them ($\frac{dP}{d\hat{t}} > 0$, blue). Such special points are called *folded singularities* (Szmolyan and Wechselberger 2001). For $\upsilon = 0.004$, we found no folded singularity in the interval $r \in [0.2 \ 0.6]$.

Studying the linear stability of the folded singularity at $F_1(r)$ gives one negative eigenvalue ($\lambda < 0$) and one positive eigenvalue ($\lambda > 0$). Hence, it is called a *folded saddle singularity FS*.

And indeed, solutions that cross the fold via the folded saddle singularity show a kind of boundary behavior: they can cross the fold with finite speed and move away from the quasi-static state (bloom) but slowly (no bloom). Such trajectories are called (singular) canards (Fig. 9). In the desingularized system (B48)–(B49) exist besides the folded saddle *FS* ($\lambda_1 < 0, \lambda_2 > 0$) folded focus *FF* (Re($\lambda_{1,2}$) < 0) at the second fold $F_2(r)$. In the case of a folded saddle *FS*, the singular canard trajectory is given by its stable manifolds.

Appendix C. More than one recurring bloom — parameter studies

The occurrence of more than one plankton bloom while thes growth rate r increases in time depends i.a. on the attack rate R_m and the mortality rate μ of the zooplankton as well as the maximum growth rate r_{max} of the phytoplankton. Of course, $r_{max} = 20$ is far from any realistic approach; nevertheless, we choose this value to evaluate how many recurring blooms can be theoretically observed for extreme high maximum growth rates.

In the following, we outline our procedure for finding the number of blooms exemplary for $r_{max} = 0.8$ (Fig. 10b, d) and different values of the attack rate R_m (Fig. 10a). (i) At first, we compute the parameter interval of R_m for which $e(\upsilon t)$ represents the unique stable state. (ii) Then, we evaluate the rate υ for which the r-coordinate of the folded saddle *FS* is equal to r_{max}. (iii) We simulate the three-dimensional TB-model (B25)–(B27) for the corresponding attack rates R_m and values of the rate υ ($P(0) = e_{3P}$, $Z(0) = e_{3Z}$ (see Table 1 for other

Fig. 10 The number of recurring blooms $P_{max} > P_b = 60$ depending on the attack rate R_m (**a**, **c**) and the mortality rate μ of the zooplankton (**b**, **d**) as well as the maximum growth rate r_{max}. Decreasing attack rate R_m and increasing mortality rate μ promote the occurrence of more and more plankton blooms during the growth rate r increases linearly in time. Parameter: $P(0) = e_P$, $Z(0) = e_Z$; others see Table 1
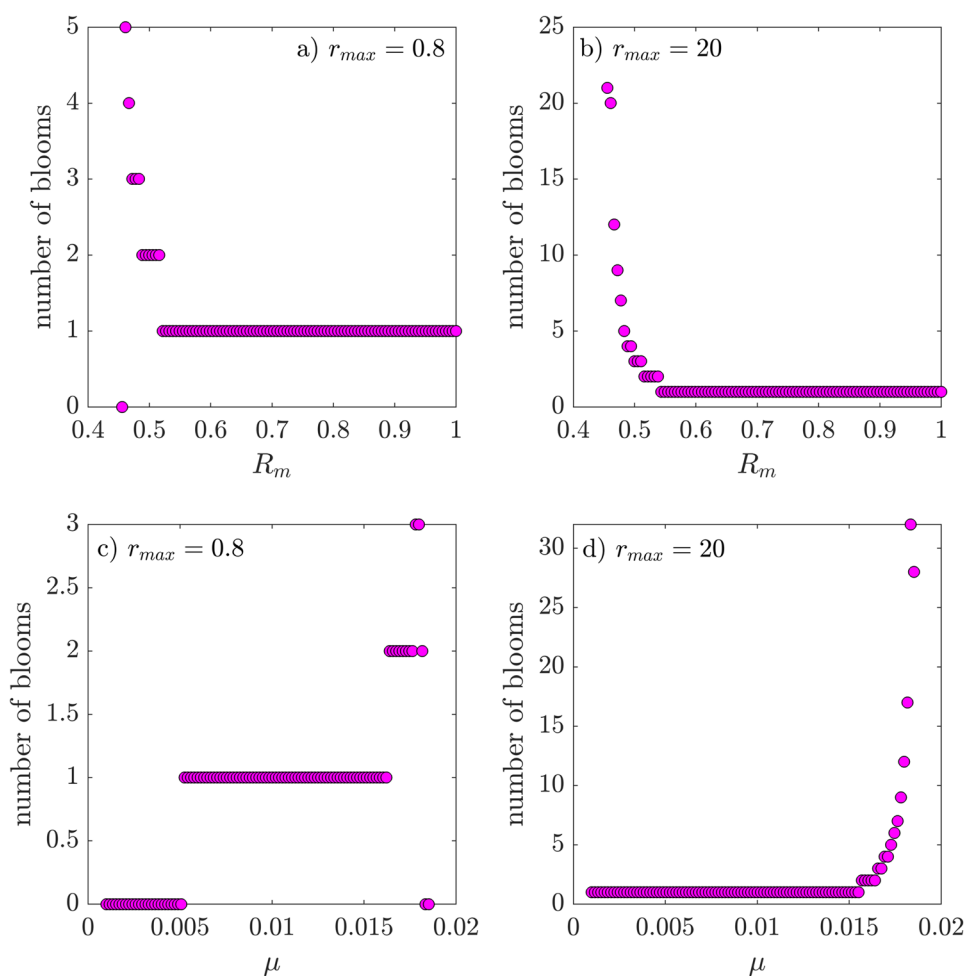
parameters). (vi) If the maximum phytoplankton density P_{max} exceeds the threshold $P_b = 60$, we increase the parameter N_b which displays the number of blooms, by one. (v) We check randomly if we have detected the correct number of blooms by visible examination of the corresponding trajectory.

Obviously, decreasing the attack rate R_m and increasing the mortality rate μ of the zooplankton cause an increase of the number of recurring blooms (Fig. 10). Hence, decreasing the predation pressure on the phytoplankton allows for more and more blooms while r increases linearly in time.

Availability of data and materials Not applicable.

Code availability Not applicable.

Declarations

Ethics approval Not applicable.

Consent to participate Not applicable.

Consent for publication Not applicable.

Competing interest The authors declare no competing interests.

References

Amaya O, Quintanilla R, Stacy BA et al (2018) Large-scale sea turtle mortality events in El Salvador attributed to paralytic shellfish toxin-producing algae blooms. Front Mar Sci 5:411

Ashwin P, Wieczorek S, Vitolo R et al (2012) Tipping points in open systems: bifurcation, noise-induced and rate-dependent examples in the climate system. Phil Trans R Soc A 370:1166–1184

Behrenfeld MJ (2010) Abandoning sverdrup's critical depth hypothesis on phytoplankton blooms. Ecology 91(4):977–989. https://doi.org/10.1890/09-1207.1

Behrenfeld MJ (2014) Climate-mediated dance of the plankton. Nat Clim Chang 4(10):880–887

Behrenfeld MJ, Boss ES (2014) Resurrecting the ecological underpinnings of ocean plankton blooms. Ann Rev Mar Sci 6:167–194

Behrenfeld MJ, Doney SC, Lima I et al (2013) Annual cycles of ecological disturbance and recovery underlying the subarctic Atlantic spring plankton bloom. Global Biogeochem Cycles 27(2):526–540

Benoît E (1981) Chasse au canard. Collect Math 31–32:37–119

Benoît E (1983) Systemes lents-rapides dans $\mathbb{R}^3$ et leur canards. Asterisque 109–110:159–191

Brøns M, Kaper T, Rotstein H (2008) Introduction to focus issue: mixed mode oscillations: experiement, computation, and analysis. Chaos 18(015):101

Busch M, Caron D, Moorthi S (2019) Growth and grazing control of the dinoflagellate Lingulodinium polyedrum in a natural plankton community. Mar Ecol Prog Ser 611:45–58

Cavender-Bares KK, Mann EL, Chisholm SW et al (1999) Differential response of equatorial Pacific phytoplankton to iron fertilization. Limnol Oceanogr 44(2):237–246

Chakraborty S, Feudel U (2014) Harmful algal blooms: combining excitability and competition. Thyroid Res 7:221–237

Chambouvet A, Morin P, Marie D et al (2008) Control of toxic marine dinoflagellate blooms by serial parasitic killers. Science 322(5905):1164,387

Coale KH, Johnson KS, Fitzwater SE et al (1996) A massive phytoplankton bloom induced by an ecosystem-scale fertilization experiment in the equatorial Pacific Ocean. Nature 383:495–501

Cullen J (1995) Status of the iron hypothesis after the open-ocean enrichment. Limnol Oceanogr 40:1336–1343

Dakos V, Matthews B, Hendry AP et al (2019) Ecosystem tipping points in an evolving world. Nat Ecol Evol 3:355–362

Desroches M, Guckenheimer J, Krauskopf B et al (2012) Mixed-mode oscillations with multiple time scales. SIAM Rev 54(2):211–288

Doney SC (2006) Plankton in a warmer world. Nature 444:695–696

Dumortier F, Roussarie R (1996) Canard cycles and Center Manifolds, 577th edn. Memories of the American Mathematical Society

Falkowski P (2012) The power of plankton. Nature 483:7–10

Field CB, Behrenfeld MJ, Randerson JT et al (1998) Primary production of the biosphere: Integrating terrestrial and oceanic components. Science 281(5374):237–240

Franks PJS (2001) Phytoplankton blooms in a fluctuating environment: the roles of plankton response time scales and grazing. J Plankton Res 23(12):1433–1441

Freund JA, Mieruch S, Scholze B et al (2006) Bloom dynamics in a seasonally forced phytoplankton-zooplankton model: Trigger mechanisms and timing effects. Ecol Complex 3(2):129–139. https://doi.org/10.1016/j.ecocom.2005.11.001

Gran H, Braarud T (1935) A quantitative study on the phytoplankton on the Bay of Fundy and Gulf of Maine (including observations on hydrography, chemistry and morbidity). J Biol Board Can 1:219–467

Griffith AW, Shumway SE, Gobler CJ (2019) Differential mortality of North Atlantic bivalve molluscs during harmful algal blooms caused by the dinoflagellate, Cochlodinium (a.k.a Margalefidinium) polykrikoides. Estuarines and Coasts 42:190–203

Guseva K, Feudel U (2020) Numerical modelling of the effect of intermittent upwelling events on plankton blooms. J R Soc Interface 14(20190):880

Hastings A, Abbott KC, Cuddington K et al (2018) Transient phenomena in ecology. Science 361:990

Hillebrand H, Brey T, Gutt J et al (2018) Climate change: warming impacts on marine Biodiversity. In: Salomon M, Markus T (eds) Handbook on marine environment protection. Springer, Cham

Hirsche HJ (2013) Long-term experiments on lifespan, reproductive activity and timing of reproduction in the Arctic copepod Calanus hyperboreus. Mar Biol 160:2469–2481

Hjerne O, Hajdu S, Larsson U et al (2019) Climate driven changes in timing, composition and magnitude of the Baltic Sea phytoplankton spring bloom. Front Mar Sci 6:482

Holling CS (1959a) Some characteristics of simple types of predation and parasitism. Can Entomol 91:385–398

Holling CS (1959b) The components of predation as revealed by a study of small mammal predation of the European pine sawfly. Can Entomol 91(5):293–320

Izhikevich EM (2007) Dynamical systems in neuroscience. MIT Press, Cambridge

Klais R, Lehtiniemi M, Rubene G et al (2016) Spatial and temporal variability of zooplankton in a temperate semi-enclosed sea: implications for monitoring design and long-term studies. J Plankton Res 38(3):652–661

Krönke J, Wunderling N, Winkelmann R et al (2020) Dynamics of tipping cascades on complex networks. Phys Rev E 101(042):311

Largier JL (2020) Upwelling bays: how coastal upwelling controls circulation, habitat, and productivity in bays. Ann Rev Mar Sci 12:415–447

Lenton TM (2020) Tipping positive change. Proc R Soc B 375(20190):123

Lenton TM, Held H, Kriegler E et al (2008) Tipping elements in the Earth's climate system. Proc Natl Acad Sci USA 105(6):1786–1793

Lewandowska AM, Boyce DG, Hofmann M et al (2014) Effects of sea surface warming on marine plankton. Ecol Lett 17(5):614–623

Lewandowska AM, Striebel M, Feudel U et al (2015) The importance of phytoplankton trait variability in spring bloom formation. ICES J Mar Sci 72:1908–1915

Mitry J, McCarthy M, Kopell N et al (2013) Excitable neurons, firing threshold manifolds and canards. J Math Neurosci 3(12)

Morel F, Rueter J, Price N (1991) Iron nutrition of phytoplankton and its possible importance in the ecology of ocean regions with high nutrient and low biomass. Oceanography 4:56–61

Morozov A, Abbott KC, Cuddington K et al (2020) Long transients in ecology: Theory and applications. Phys Life Rev 32:1–40

O'Keeffe PE, Wieczorek S (2020) Tipping phenomena and points of no return in ecosystems: Beyond Classical Bifurcations. SIAM J Appl Dyn Syst 19(4):2371–2402

O'Sullivan E, Mulchrone K, Wieczorek S (2022) Rate-induced tipping to metastable zombie fires. arXiv preprint arXiv:2210.02376

Parmesan C (2006) Ecological and evolutionary responses to recent climate change. Annu Rev Ecol Evol Syst 37:637–669

Perryman C, Wieczorek S (2014) Adapting to a changing environment: non-obvious thresholds in multi-scale systems. Proc R Soc A Math Phys Eng Sci 470(2170):20140,226

Pinek L, Mansour I, Lakovic M et al (2020) Rate of environmental change across scales in ecology. Biol Rev 95:1798–1811

Richards KJ (2017) Viral infections of oceanic plankton blooms. J Theor Biol 412:27–35

Riley G (1946) Factors controlling phytoplankton populations on Georges Bank. J Mar Res 6:54–73

Riley G, Stommel H, Bumpus D (1949) Quantitative ecology of the plankton of the western North Atlantic. Bulletin of the Bingham Oceanographic Collection 12:1–169

Rumyantseva A, Henson S, Martin A et al (2019) Phytoplankton spring bloom initiation: The impact of atmospheric forcing and light in the temperate North Atlantic Ocean. Prog Oceanogr 178(102):202

Scheffer M, Carpenter S, Foley JA et al (2001) Catastrophic shifts in ecosystems. Nature 413:591–596

Simpson JH, Sharples J (2012) Introduction to the physical and biological oceanography of shelf seas. Cambridge University Press, New York

Smith SJ, Edmonds J, Hartin CA et al (2015) Near-term acceleration in the rate of temperature change. Nat Clim Chang 5:333–336

Sommer U, Lewandowska AM (2011) Climate change and the phytoplankton spring bloom: warming and overwintering zooplankton have similar effects on phytoplankton. Glob Chang Biol 17(1):154–162

Sommer U, Adrian R, De Senerpont Domis L et al (2012) Beyond the plankton ecology group (PEG) model: Mechanisms driving plankton succession. Annu Rev Ecol Evol Syst 43:429–448

Sverdrup H (1953) On conditions for the vernal blooming of phytoplankton. ICES J Mar Sci 18(3):287–295

Szmolyan P, Wechselberger M (2001) Canards in $\mathbb{R}^3$. J Differ Equ 177:419–453

Trombetta T, Vidussi F, Mas S et al (2019) Water temperature drives phytoplakton blooms in coastal waters. PLoS ONE 14(4):e0214933

Truscott J, Brindley J (1994) Ocean plankton populations as excitable media. Bull Math Biol 56(5):981–998

Uye S (1986) Impact of copepod grazing on the red tide flagellate. Mar Biol 92:35–43

Vanselow A, Wieczorek S, Feudel U (2019) When very slow is too fast - collapse of a predator-prey system. J Theor Biol 479:64–72

Velo-Suárez L, Brosnahan ML, Anderson DM et al (2013) A quantitative assessment of the role of the parasite Amoebophrya in the termination of Alexandrium fundyense blooms with a small coastal embayment. PLoS ONE 8(12):e81,150

Wake G (1991) Picoplankton and marine food chain dynamics in a variable mixed layer: a reaction-diffusion model. Ecol Model 57:193

Walther GR, Post E, Convey P et al (2002) Ecological responses to recent climate change. Nature 416:389–395

Wechselberger M, Mitry J, Rinzel J (2013) Canard theory and excitability. In: Kloeden PE, Pötzsche C (eds) Nonautonomous Dynamical Systems in the Life Sciences. Springer, pp 89–133

Wieczorek S, Ashwin P, Luke C et al (2011) Excitability in ramped systems: the compost-bomb instability. Proc R Soc Lond Ser A 467:1243–1269

Wieczorek S, Xie C, Ashwin P (2021) Rate-induced tipping: Thresholds, edge states and connecting orbits. arXiv preprint arXiv:2111.15497

Winder M, Berger SA, Lewandowska A et al (2012) Spring phenological responses of marine and freshwater plankton to changing temperature and light conditions. Mar Biol 159:2491–2501